

HYDRODYNAMICS CIRCULATION MODEL IN THE ESTUARY OF PALU RIVER BASED ON NUMERICAL CALCULATIONS

MOHAMMAD LUTFI

Department of Petroleum Engineering, STT MIGAS,
No. 76 Jalan Transad, 76127, Balikpapan, Indonesia
E-mail: lutfi_plhld@yahoo.co.id

Abstract

Early warning system based on numerical models is important in disaster mitigation to reduce economic and human losses. A hydrodynamics circulation model and the causes of its failures in the Palu River Estuary were discussed in this article using ECOMSED and GIS analysis. The investigation revealed that the morphology of the estuary at the river mouth and bathymetry has caused the sigma coordinate system difficult to be applied. This problem can be solved by setting input data such as time space resolution, discharge, and water elevation such that the model setup meets the requirements of the CFL criteria. The results showed that current simulations for one tidal cycle at minimum and maximum discharges move out of the river, it revealed that the estuary is dominated by river discharges. The estuary is classified as a highly stratified estuary based on simulations of the distribution of salinity and temperature on a vertical cross-section. Verification of water elevation, direction and current velocity, distribution of salinity and temperature was performed using field observation and secondary data, where the results revealed a good agreement.

Keywords: ECOMSED, GIS, Hydrodynamics, Numerical modeling, Palu River.

1. Introduction

Disasters are certainty, but when, where, and how large its impact is uncertainty before the disaster occurs. Mitigation is an approach to answer these questions as an effort to reduce economic and human losses [1].

Multiple hazards triggered by the earthquake that took place simultaneously on September 28th, 2018 in Palu city, Sulawesi have attracted the attention of many researchers in the world to study the morphology and hydrodynamics of Palu Bay. Field observation revealed that subsidence [2] and tsunami [3, 4] occurred along the coast.

The numerical method is one of the approaches in disaster mitigation in the coastal area. It can be used for monitoring water quality [5], flood control management [6], and hydrometeorology disaster forecast [7-9]. The accuracy of numerical models is very dependent on the selection of the model used and complex natural variability as input data into the model. Therefore, the numerical model and the input data chosen should be reliable to be used for prediction of the past, present, and future.

Geological and geophysical factors are obstacles to generalising specific finding in the Palu disaster [10]. Numerical simulation in previous research [11] was carried out by modifying bathymetry data without explaining the causes of numerical failure comprehensively, so that understanding of other simulation scenarios cannot be explained.

According to the unique morphology of Palu River Estuary and the stability of numerical calculations above, the objective of this present research was to simulate hydrodynamics circulation and to investigate the causes of numerical simulation failures in the estuary of Palu River, so that a better prediction can be achieved.

2. Methods

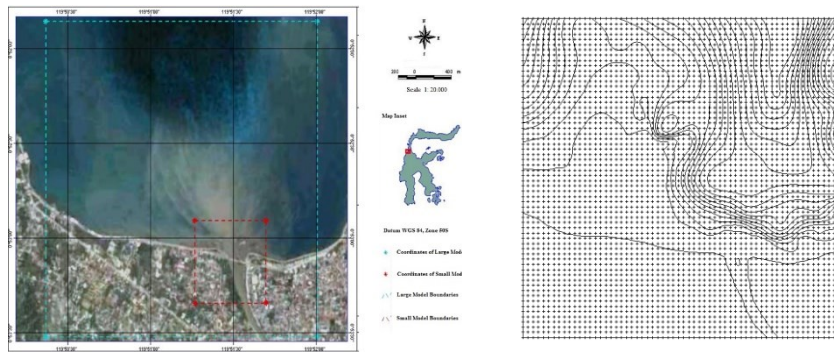
The prediction of hydrodynamics circulation in the Palu River Estuary was carried out using the computer programme. Figure 1(a) shows the computational domain, where the area comprises the small part of the Palu Bay and the small part of the Palu River.

The finite difference method is used for numerical calculation, where the horizontal finite difference mesh of 125×125 grids squares, equally spaced at 25 m intervals, and vertical grids of 11 σ -levels. Figure 1(b) shows the grid model, shoreline, and bathymetry contour of the study area.

Depth interpolation was conducted using GIS software. At this stage the topography map, sea map, and satellite imagery were digitized to obtain geometrically corrected coastline and bathymetry data, then the output is used as a lateral and open boundaries condition on the model.

River discharge is used as a boundary condition at the upstream of the river in the simulation area. It is assumed to be constant throughout the simulation which is equal to $2 \text{ m}^3/\text{s}$ and $36 \text{ m}^3/\text{s}$ obtained from measurement data in the field to represent minimum and maximum discharge conditions, while for verification purposes of tidal currents, simulation was run without the influence of discharge. The temperature and salinity at the upstream of the river and the open boundaries in the sea are 28°C , 0 ppt, 29°C , and 30 ppt respectively. 6 Tidal constants (S_2 , M_2 , N_2 , K_1 , P_1 and O_1) at the Palu Bay are used as input data at the open boundary of

the sea, while the results of interpolation of river depth and bathymetry are used as lateral and lower boundaries.



(a) Map of simulation area.

(b) Model grid (finite difference scheme).

Fig. 1. Model setup.

Investigation of the causes of simulation failure was performed by modifying the parameters of time step, grids, water depth, discharge, and tidal data. Once the error problem has been resolved, then hydrodynamics numerical model runs smoothly.

In this research, ECOMSED is used to analyse hydrodynamics circulation in the Palu River Estuary. This model has been widely used in the estuary and the ocean, [12-19]. The governing equation of ECOMSED used in this model is a continuity equation, Reynold momentum equation, temperature and salinity conservation equation, and turbulence equations that have been transformed into the sigma coordinate system to obtain accurate approximations of the bottom and surface mixing layers [20].

Continuity equation is:

$$\frac{\partial DU}{\partial x} + \frac{\partial DV}{\partial y} + \frac{\partial \omega}{\partial \sigma} + \frac{\partial \zeta}{\partial t} = 0 \tag{1}$$

The Reynolds momentum equations are as follows:

$$\begin{aligned} & \frac{\partial DU}{\partial t} + \frac{\partial U^2 D}{\partial x} + \frac{\partial DUV}{\partial y} + \frac{\partial U\omega}{\partial \sigma} - fvD + gD \frac{\partial \zeta}{\partial x} \\ & = \frac{\partial}{\partial \sigma} \left(\frac{K_M}{D} \frac{\partial U}{\partial \sigma} \right) \frac{gD^2}{\rho_0} \frac{\partial}{\partial x} \frac{\partial \rho}{\partial \sigma} + \frac{gD}{\rho_0} \frac{\partial D}{\partial x} \frac{\partial \rho}{\partial \sigma} \frac{\partial \rho}{\partial \sigma} + F_x \end{aligned} \tag{2}$$

$$\frac{\partial DV}{\partial t} + \frac{\partial DUV}{\partial x} + \frac{\partial V^2 D}{\partial y} + \frac{\partial v\omega}{\partial \sigma} - fuD + gD \frac{\partial \zeta}{\partial y}$$

$$= \frac{\partial}{\partial \sigma} \left(\frac{K_M}{D} \frac{\partial V}{\partial \sigma} \right) \frac{gD^2}{\rho_0} \frac{\partial}{\partial y} \int \rho \partial \sigma + \frac{gD}{\rho_0} \frac{\partial D}{\partial y} \int \sigma \frac{\partial \rho}{\partial \sigma} \partial \sigma + F_y \quad (3)$$

$$\rho g = \frac{-\partial P}{\partial Z} \quad (4)$$

where A is the Coriolis parameter, K_M is the vertical eddy diffusivity of turbulent momentum mixing, P is the pressure, g is the gravitational acceleration, ρ is the reference density, ρ_0 is the in situ density, F_x and F_y represent the terms of horizontal mixing processes.

The conservation equations of salinity and temperature could be written as follows

$$\frac{\partial DS}{\partial t} + \frac{\partial DUS}{\partial x} + \frac{\partial SVD}{\partial y} + \frac{\partial S\omega}{\partial \sigma} = \frac{\partial}{\partial \sigma} \left(\frac{K_H}{D} \frac{\partial S}{\partial \sigma} \right) + F_S \quad (5)$$

$$\frac{\partial DT}{\partial t} + \frac{\partial DUT}{\partial x} + \frac{\partial \theta VD}{\partial y} + \frac{\partial T\omega}{\partial \sigma} = \frac{\partial}{\partial \sigma} \left(\frac{K_H}{D} \frac{\partial T}{\partial \sigma} \right) + F_T \quad (6)$$

where θ , S , and K_H are the in situ temperature, the salinity, and the vertical eddy diffusivity for turbulent mixing of heat and salt respectively.

According to the user's manual of ECOMSED [21], the turbulence closure may be written as follows

$$\frac{\partial q^2 D}{\partial t} + \frac{\partial Uq^2 D}{\partial x} + \frac{\partial Vq^2 D}{\partial y} + \frac{\partial \omega q^2}{\partial z} = \frac{\partial}{\partial \sigma} \left(\frac{K_q}{D} \frac{\partial q^2}{\partial \sigma} \right) \quad (7)$$

$$+ \frac{2K_M}{D} \left[\left(\frac{\partial U}{\partial \sigma} \right)^2 + \left(\frac{\partial V}{\partial \sigma} \right)^2 \right] + \frac{2g}{\rho_0} K_H \frac{\partial \rho}{\partial \sigma} \frac{2Dq^3}{B_1 l} + F_q$$

$$\frac{2(q^2 l D)}{\partial t} + \frac{\partial (Uq^2 l D)}{\partial x} + \frac{\partial (Vq^2 l D)}{\partial y} + \frac{\partial (\omega q^2 l)}{\partial \sigma} = \frac{\partial}{\partial \sigma} \left(\frac{K_q}{D} \frac{\partial (q^2 l)}{\partial \sigma} \right) \quad (8)$$

$$+ l E_1 \left\{ \frac{K_M}{D} \left[\left(\frac{\partial U}{\partial \sigma} \right)^2 + \left(\frac{\partial V}{\partial \sigma} \right)^2 \right] + \frac{qD^3}{\rho_0} K_H \frac{\partial \rho}{\partial \sigma} \right\} - \frac{Dq^3}{B_1} \tilde{W} + F_l$$

Model verification was performed using field data and tidal data from DISHIDROS. Measurements were taken at three locations (station A, station B, and station C). The stations are located along the estuary, which are placed from the river mouth to the upstream of the river. The distance of each station is as follows: Station A is located at the river mouth, station B is located 125 m from station A, and station C is located 250 m from station A. At each station, measurements are taken for depth, salinity, discharge, temperature, and salinity. Measurement of temperature and salinity was conducted for 3 points vertically (on the near surface, middle, and near bottom), whereas the direction and current velocity measurements were carried out only at station A. Based on the

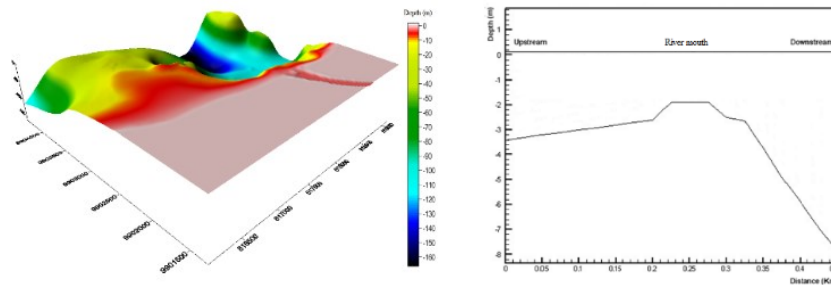
measurements, the simulation on the vertical profile is focused on the upstream up to the downstream, where in that interval the currents velocity, temperature, and salinity measurements were carried out.

3. Results and Discussion

3.1. Depth interpolation

The kriging interpolation method was used to reveal the river depth and the bathymetry. Figure 2(a) shows that the maximum bathymetry depth of the simulation area is 167.83 m, where in the east is steeper than in the west. Figure 2(b) shows that the Palu River is categorized as a shallow river, where the water depth from upstream to the mouth of the river ranging from 1.9 m to 3.5 m.

The steepness in the east has the potential to cause underwater landslides if the sediment from the river that enters into the Palu Bay has not been strongly consolidated so that it collapses and landslides during an earthquake, then triggers a tsunami. these results are consistent with Muhari's hypothesis [22]. If a tsunami occurs outside the bay, then the wave energy coming from the Makassar strait into the Palu Bay will be concentrated and amplified with a steep bathymetry so that it can cause large differences between the tidal in the open ocean (Makassar strait) and nearshore at estuary of Palu River.



(a) Three dimensional model of bathymetry.

(b) Vertical cross section of the river depth.

Fig. 2. Simulation results of the depth interpolation.

3.2. Run time error analysis

Run time errors occurred during simulation. The problem of numerical instability is caused by the non-linear phenomena. The simulation results show that the ECOMSED programme can run stable if the advection term is linearized to simplify problems in numerical calculations, the mathematical equation can be represented in elementary functions so that it can be solved analytically [23].

The advection term in the momentum equation represents changes in physical parameters over time space. Therefore, by not considering the advection term in the momentum equation, the hydrodynamic circulation in the Palu River Estuary will not be well described, especially in the shallow waters and surrounding structures.

3.2.1. Horizontal grid Size and maximum Depth

Simulation results reveal that the ECOMSED becomes unstable if the simulation area has a larger horizontal grid size compared to the depth of the sea at the open boundary. The maximum depth at the open boundary is 167.83 meters, while the horizontal grid size is only 25 m. If the area of the simulation is enlarged, the horizontal grid size should be reduced and the simulation time will run longer.

The wave in the Palu Bay is categorized as long wave, where the maximum grid width is one quarter of the wavelength, whereas the maximum width of the grid is one third of the minimum width of the Palu River in the model domain. based on this criterion, the model at the open boundary has a high resolution, while the upstream has a lower resolution.

3.2.2. Steep bathymetry of the model domain

The simulation area has a steep bathymetry at a depth of 10 m to a maximum depth of 167.83 m. The depth interpolation was conducted for a maximum depth of 10 m in the model domain, where the result revealed that simulation was running stable. However, run time error occurs during simulation if the maximum depth was imposed at the open boundary is 20 m. It reveals that the steepness between 10 m to 20 m causes numerical model instability.

3.2.3. Limitation of the sigma coordinate system

Numerical experiment was conducted on the vertical cross section by setting vertical grids. The results revealed that run time error occurred faster for 7 σ -levels compared to 11 σ -levels. It revealed that the grid resolution was not enough due to rapidly varying bathymetry. The addition of the σ -levels in this case increases the duration of the simulation but does not solve the error problem.

3.2.4. Shallow waters at the river mouth

Simulation result revealed that numerical instability occurs when the amplitude is greater than the minimum depth at the river mouth around the delta. Therefore, the river depth must be added such that the minimum water depth greater than the tidal amplitude.

Figure 3(a) shows the condition of the Palu River mouth before the disaster and Fig. 3(b) after a disaster. Both figures show the water depth at the river mouth is relatively the same so that the addition of the water depth for shallow areas must still be done based on criteria of depth specified in model grid [24].

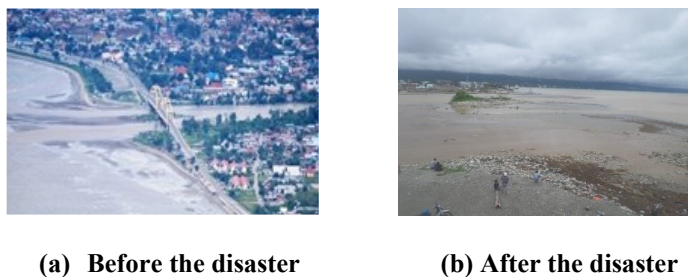


Fig. 3. The condition of the Palu River mouth.

3.2.5. Maximum discharge

Three simulations with different scenarios revealed that discharge is also one of the causes of numerical instability. Run time error occurred for discharge of 36 m³/s. whereas the simulation for discharge of 2 m³/s run smoothly. It reveals that large discharge in this model cannot be applied without modifying bathymetry data. Therefore, the latest bathymetry data is needed to apply this model under these conditions.

The numerical stability is strongly influenced by the Friedrich Levy's Courant (CFL) Criteria [25] in equation (9)

$$\Delta t_E \leq \frac{1}{C_t} \left| \frac{1}{\partial x^2} + \frac{1}{\partial y^2} \right|^{-\frac{1}{2}} \quad (9)$$

where $C_t = 2 (gH)^{1/2} + U_{max}$; U_{max} is the maximum velocity.

Equation (9) shows that the choice of time step is influenced by the size of the horizontal grid, the maximum depth, the acceleration of the earth's gravity and the maximum velocity. The maximum time step for the internal mode in this study is $t < 8.9$ s and for the external model is $t < 0.22$ s.

The next experiment revealed that the smaller the time steps taken, the longer simulation goes. Figure 4(a) shows run time error for $\Delta t = 5$ s and Fig. 4(b) shows run time error for $\Delta t = 1$ s. It reveals that there were no significant changes by reducing the time step.

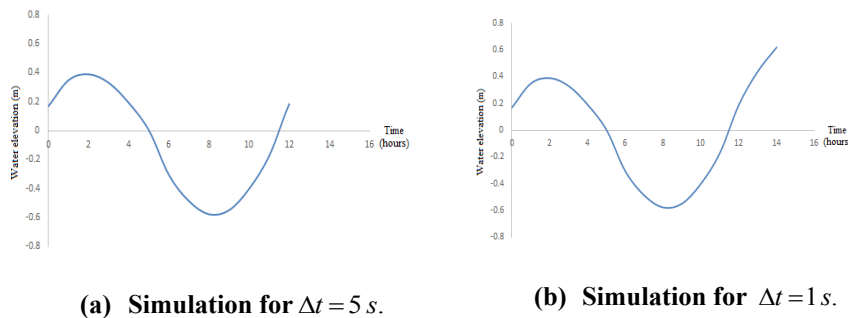


Fig. 4. Simulation results of water elevation.

3.3. Current model

Tidal currents move in opposite directions at slack low water and slack high water in narrow and closed waters such as bay, so that the velocity period follow the tidal period that generates it. The tidal current pattern corresponds well to the results of previous studies conducted at Jakarta bay [26] and at the Ariake sea [27].

The current velocity at slack low water and slack high water ranging from 0 m/s to 0.027 m/s and the minimum current velocity occurs during the ebb and flood conditions, where the current velocity ranging from 0 m/s to 0.007 m/s as shown in Fig. 5. Surface current simulation for discharge of 36 m³/s. Figure 6 shows the

pattern of surface current at ebb and flood condition moves out of the river. Based on the direction and current velocity in the two simulations, it can be concluded that the effect of tides on the Palu River Estuary is relatively small compared to river discharge.

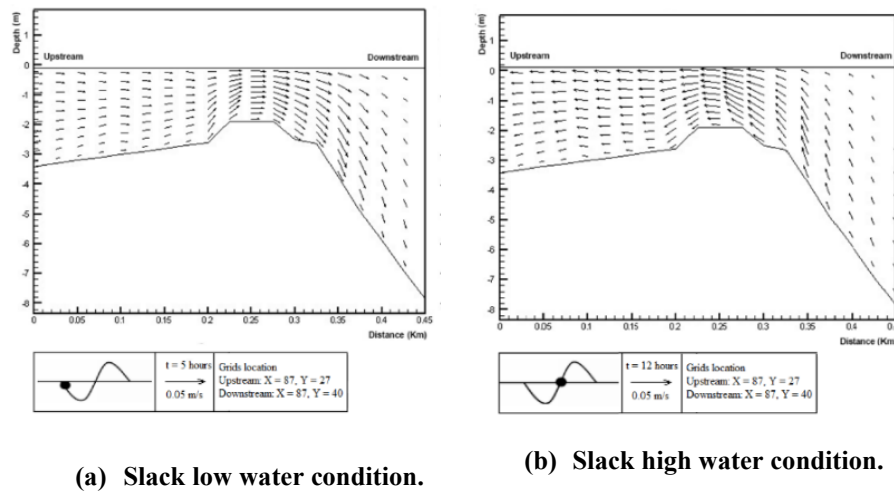


Fig. 5. Current model on the vertical cross section for $Q = 0 \text{ m/s}^3$.

3.4. Comparison of simulation results and field data for water elevation and current velocity`

The type of tides in a waters can be determined by calculating the Formzahl value (F) [28]. The waters at Palu Bay is categorized as mixed tide prevailing semidiurnal based on the calculation ($F = 0.29$), where at ebb and flood occurs twice a day with a time difference between the highest peaks. Figure 7(a) shows the simulation result of ECOMSED for water elevation, where the flood condition was 269.2 cm and ebb condition was 22.6 cm, while the DISHIDROS prediction shows that the flood condition was 263.2 cm and the ebb condition was 31.4 cm. The amplitude of ECOMSED is greater than DISHIDROS prediction, the difference is caused by differences in tidal harmonic constants input data in the two models.

Figure 6(b) shows that the field observation for current velocity is greater than simulation results. This is caused by adding depth to the simulation area to avoid the failure of numerical calculations. The waters depth for the simulation at ebb condition was 1.3 m and the flood was 2.5 m, while the waters depth for field data at ebb was 0.54 m and the flood was 1.03 m.

Overall, the water elevation verification results show a consistent pattern between ECOMSED and prediction from DISHIDROS based on the admiralty method [29] with a root mean square error (RMSE) [30] of about 0.114 and the pattern of the current velocity for the simulation results corresponds well to the field data. Based on the verification results, this model is feasible to be applied for the prediction of hydrodynamics in this area.

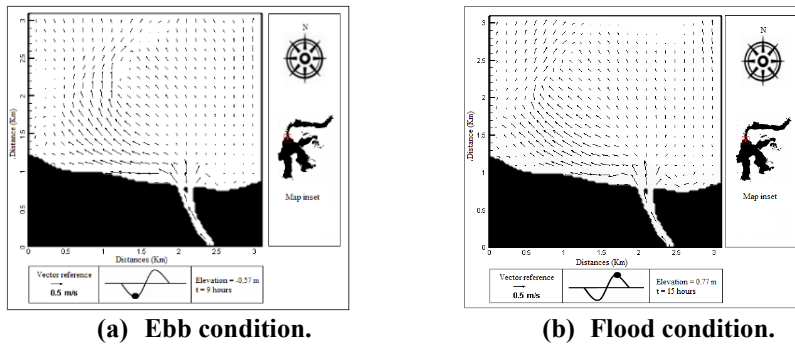


Fig. 6. Current model on the horizontal cross section for $Q = 36 \text{ m}^3/\text{s}^3$.

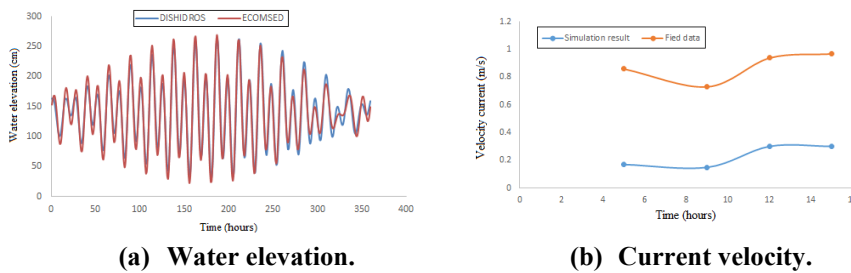


Fig. 7. Comparison of simulation results and data field.

3.5. Temperature distribution model

The temperature distribution on the vertical cross section for ebb condition is homogeneous from surface to bottom as shown in Fig. 8(a), while Fig. 8(b) shows a small variation at the lowest layer for flood condition. There is no variation at the surface layer because of the turbulence. At flood condition, the temperature increases with the depth of the water. This is caused by the effect of sea water temperature which is hotter than the temperature of river water that moves at the lower layer of fresh water. At lowest water and highest water conditions, the difference in water temperature at the top layer to the lowest layer was 0.9°C , where the minimum temperature was 28.05°C and the maximum temperature was 28.95°C . The results are in accordance with previous studies, where the temperature difference under these conditions is not more than 1°C [31].

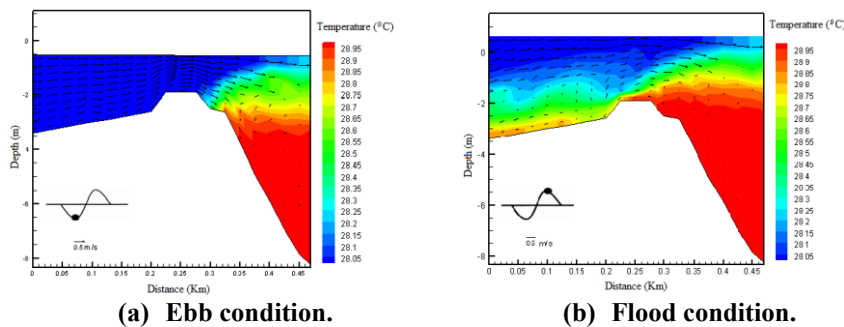


Fig. 8. Temperature patterns on the vertical cross section.

3.6. Salinity distribution model

Sea water propagation into the upstream of the river depends on the discharge. The greater the river discharge the shorter the distance of sea water reach upstream [32]. Figure 9 shows that at ebb and flood conditions, the sea water enters upstream with a maximum salinity of 34 ppt for a discharge of 2 m³/s, while for discharge of 36 m³/s, the maximum salinity at the upstream was 0 ppt at ebb condition and 24 ppt for flood condition as shown in Fig. 10.

Based on the simulation results, the Palu River Estuary is classified as a highly stratified estuary, where discharge is greater than tidal effect [33]. In this condition, freshwater and saltwater separate, but the river discharge of 36 m³/s is not strong enough to push the whole salt water back into the sea, so that the salt water will be under fresh water because the saltwater density is greater than freshwater.

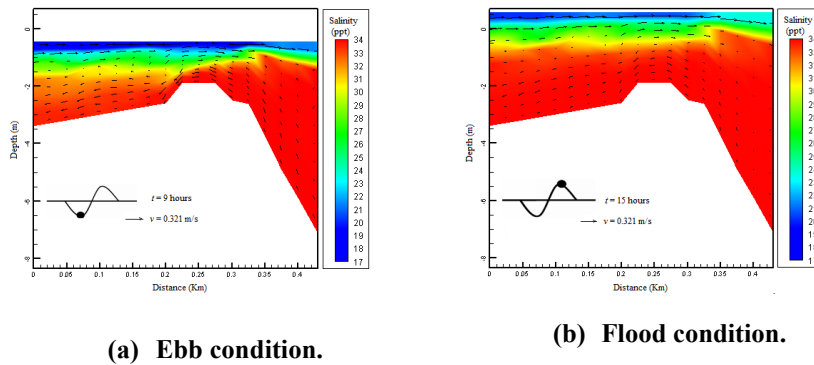


Fig. 9. Overlay of current and salinity patterns on the vertical cross section for ebb and flood conditions ($Q = 2 \text{ m}^3/\text{s}$).

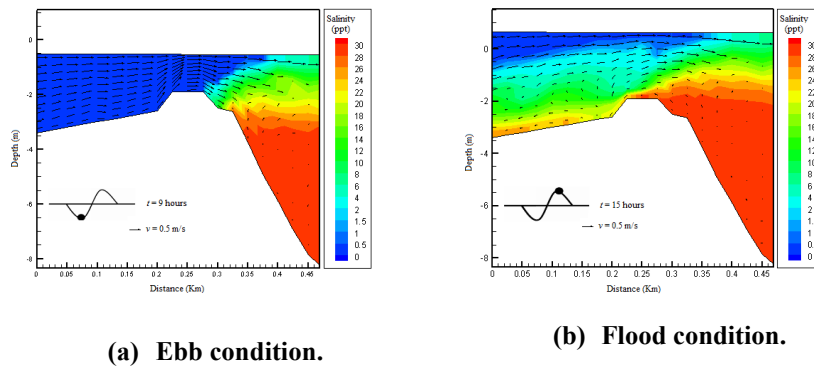


Fig. 10. Overlay of current and salinity patterns on the vertical cross section for ebb and flood conditions ($Q = 36 \text{ m}^3/\text{s}$).

3.7. Model verification of temperature and salinity

Tables 1 and 2 show a good agreement between simulation results and field data at all stations. Small variations between measurements and simulations are caused by

differences in river depth between the model and field data. The difference is seen only in the middle and near bottom layers, whereas in the near surface is exactly the same.

Table 1. Comparison of field data and simulations result of temperature.

Time (hours)	Station A (field data)			Station A (simulation)		
	Near surface (°C)	Middle (°C)	Near bottom (°C)	Near surface (°C)	Middle (°C)	Near bottom (°C)
5	28	28	28	28	28	28.1
9	28	28	28	28	28	28
12	28	28	28	28	28	28
15	28	28	28	28.1	28.6	28.9

Time (hours)	Station B (field data)			Station B (simulation)		
	Near surface (°C)	Middle (°C)	Near bottom (°C)	Near surface (°C)	Middle (°C)	Near bottom (°C)
5	28	28	28	28	28	28.1
9	28	28	28	28	28	28
12	28	28	28	28	28	28
15	28	28	28	28	28.1	28.3

Time (hours)	Station C (field data)			Station C (simulation)		
	Near surface (°C)	Middle (°C)	Near bottom (°C)	Near surface (°C)	Middle (°C)	Near bottom (°C)
5	28	28	28	28	28	28.1
9	28	28	28	28	28	28
12	28	28	28	28	28	28
15	28	28	28	28	28.1	28.3

Table 2. Comparison of field data and simulation result of salinity.

Time (hours)	Station A (field data)			Station A (simulation result)		
	Near surface (ppt)	Middle (ppt)	Near bottom (ppt)	Near surface (ppt)	Middle (ppt)	Near bottom (ppt)
5	0	0	1	0	0.5	1
9	0	0	0	0	0	0
12	0	0	0	0	0	0
15	0	0	3	0	2	4

Time (hours)	Station B (field data)			Station B (simulation result)		
	Near surface (ppt)	Middle (ppt)	Near bottom (ppt)	Near surface (ppt)	Middle (ppt)	Near bottom (ppt)
5	0	0	3	0	0.5	4
9	0	0	0	0	0	0
12	0	0	1	0	0	1
15	0	3	15	0	3	17

Time (hours)	Station C (field data)			Station C (simulation result)		
	Near surface (ppt)	Middle (ppt)	Near bottom (ppt)	Near surface (ppt)	Middle (ppt)	Near bottom (ppt)
5	0	0	2	0	0	3
9	0	0	0	0	0	0
12	0	0	0	0	0	0
15	0	0	10	0	1	9

4. Conclusions

Three dimensional hydrodynamics circulation model has been made using ECOMSED to predict water elevation, current, temperature and salinity distribution in the Palu River Estuary and GIS analysis is used to investigate the causes of numerical calculation failures.

According to the simulation results, the morphology of the estuary at the river mouth and bathymetry has caused the sigma coordinate system difficult to be applied. This problem can be solved by setting input data such as time space resolution, discharge, and water elevation such that the model set-up meets the requirements of the CFL criteria. The results showed that current simulations for one tidal cycle at minimum and maximum discharges move out of the river, it revealed that the estuary is dominated by river discharges. The estuary is classified as a highly stratified estuary based on simulations of the distribution of salinity and temperature distribution on a vertical cross-section. Verification of direction and current velocity, distribution of salinity and temperature was performed using field observation, while the water elevation with data from DISHIDROS, where the results revealed a good agreement.

Investigation of the causes of simulation failures is difficult to be done because of the ECOMSED and GIS software are run separately, so it takes a long time to make the simulation run smoothly. Therefore, ECOMSED and GIS software need to be integrated. By conducting further studies with a comprehensive simulation, this model is expected to be used to reveal the impact of environmental damage before, after, and when a disaster occurs by changing the input data into the model.

Acknowledgement

I thank the IDEC, Hiroshima University for supporting the simulation at the Coastal Hazards and Energy System Science Laboratory and I express my gratitude to Prof. Yamashita, Dr. Mishima, Dr. Lee, and Drs. Mardeli for fruitful discussions.

Nomenclatures

A	Coriolis parameter
F	Formzahl value
F_x, F_y, F_θ, F_q	Represent the terms of horizontal mixing processes
g	Gravitational acceleration, m/s ²
H	Water depth, m
K_M	Vertical eddy diffusivity of turbulent momentum mixing
l	Turbulence for macro scale
P	Pressure, Pa
Q	Discharge, m/s ³
q	Turbulence component
S	Salinity, ppt
U, V, W	Components of the current velocity, m/s

Greek Symbols	
θ	In situ temperature, °C
ζ	Water elevation, m
ρ	In situ density, kg/m ³
ρ_0	Reference density, kg/m ³
w	Vertical velocity, m/s
Abbreviations	
CFL	Courant Friedrichs Levy
DISHIDROS	Dinas hidrooseanografi (hydro oceanographic office)
DTE	External mode time step
DTI	Internal mode time step
ECOMSED	Estuary coastal ocean model and sediment transport
GIS	Geographical information system
IDEC	International development and cooperation
RMSE	Root mean square error

References

1. Hermon, D. (2019). Evaluation of physical development of the coastal tourism regions on tsunami potentially zones in Pariaman City-Indonesia. *International Journal of GEOMATE*, 17(59), 189-196.
2. Arikawa, T.; Muhari, A.; Okumura, Y.; Dohi, Y.; Afriyanto, B.; Sujatmiko, K.A.; and Imamura, F. (2018). Coastal subsidence induced several tsunamis during the 2018 Sulawesi earthquake. *Journal of Disaster Research*, 13, 1-3.
3. Umar, M.; Margaglio, G.; and Fitrayansyah, A. (2019). Post-tsunami survey of the 28 September 2018 tsunami near Palu Bay in Central Sulawesi, Indonesia: Impacts and challenges to coastal communities. *International Journal of Disaster Risk Reduction*, 38, 101229.
4. Omira, R.; Dogan, G.G.; Hidayat, R.; Husrin, S.; Prasetya, G.; Annunziato, A.; Proietti, T.; Probst, P.; Paparo, M.A.; Wronna, M.; Zaytsev, A.; Pronin, P.; Giniyatullin, A.; Putra, P.S.; Hartanto, D.; Ginanjar, G.; Kpngko, W.; Pelinovsky, E.; and Yalciner, A.C. (2019). The September 28th, 2018, Tsunami in Palu-Sulawesi, Indonesia: A Post-Event Field Survey. *Pure and Applied Geophysics*, 176, 1379-1395.
5. Chanudet, V.; Smits, J.; Van Beek, J.; Boderie, P.; Guérin, F.; Serça, D.; Deshmukh, C.; and Descloux, S. (2016). Hydrodynamic and water quality 3D modelling of the Nam Theun 2 Reservoir (Lao PDR): predictions and results of scenarios related to reservoir management, hydrometeorology and nutrient input. *Hydroécologie Appliquée*, 19, 87-118.
6. Tyree, J.; Ven, J.S.; Pascua, M.C.; Rahaman, M.M.; Tenorio, A.L; and Lutfi, M. (2013). Effectiveness of camanava flood control project: A case study of selected flood control structures during typhoon gener and monsoon rains in August 2012. *Journal of International Development and Cooperation*, 19(3), 131-45.
7. Thakur, P.K.; Aggarwal, S.P.; Dhote, P.; Nikam, B.R.; Garg, V.; Bhatt, C.M.; Chouksey, A.; and Jha, A. (2019). Hydrometeorological hazards mapping,

- monitoring and modelling. *Remote Sensing of Northwest Himalayan Ecosystems*, 139-169.
8. Wang, P.; Li, X.; Tong, Y.; Huang, Y.; Yang, X.; and Wu, X. (2019). Vegetation dynamics dominate the energy flux partitioning across typical ecosystem in the Heihe River basin: Observation with numerical modeling. *Journal of Geographical Sciences*, 29(9), 1565-1577.
 9. Varlas, G.; Anagnostou, M.; Spyrou, C.; Papadopoulos, A.; Kalogiros, J.; Mentzafou, A.; Michaelides, S.; Baltas, E.; Karymbalis, E.; and Katsafados, P. (2019). A multi-platform hydrometeorological analysis of the flash flood event of 15 November 2017 in Attica, Greece. *Remote Sensing*, 11(1), 45.
 10. Goda, K.; Mori, N.; Yasuda, T.; Prasetyo, A.; Muhammad, A.; and Tsujio, D. (2019). Cascading geological hazards and risks of the 2018 Sulawesi Indonesia earthquake and sensitivity analysis of tsunami inundation simulations. *Frontiers in Earth Science*, 7, 1-16.
 11. Lutfi, M.; Afifah, R.S.; Sulaiman, B.; and Risna. (2018). Numerical simulation of hydrodynamic for abrupt bathymetry in estuary of Palu River. *Indian Journal of Science and Technology*, 11(23), 1-5.
 12. Kusuhaba, K.; Sakuraba, M.; Onaka, S.; Ichikawa, S.; and Awazu, Y. (2019). Channel and basin sedimentation modelling under limited data availability: Case study of a port in eastern Africa. *Proceedings of the International Conference on Asian and Pacific Coasts*, Springer, Singapore, 449-455.
 13. Kang, J.; Wang, Y.; Xu, J.; Yang, S.; and Hou, H. (2019). A Mesh reduced method for speeding up structured grid-based water quantity and quality models in large-scale River Networks. *Water*, 11(3), 437.
 14. Liu, Y.; Bao, A.; Chen, X.; and Zhong, R. (2019). A Model study of the discharges effects of Kaidu River on the salinity structure of Bosten Lake. *Water*, 11(1), 8.
 15. Gao, J.; Zhu, D.; Wu, G.; Hu, B.; and Huang, H. (2019). Tidal and tidal current characteristics in the Guangxi Gulf of Tonkin, South China Sea. *Ocean Dynamics*, 69(9), 1037-1051.
 16. Nie, H.; Sun, Z; and Xie C. (2012). Simulating a typhoon storm surge using a nested ECOMSED model. *Procedia Engineering*, 31, 775-780.
 17. Xu, T.P.; Zhang, M.L.; Jiang, H.Z.; Tang, J.; Zhang, H.X.; and Qiao, H.T. (2019). Numerical investigation of the effects of aquatic plants on wind-induced currents in Taihu Lake in China. *Journal of Hydrodynamics*, 31(4), 778-787.
 18. Lai, Y.G.; and Wu, K. (2019). A Three-dimensional flow and sediment transport model for free-surface open channel flows on unstructured flexible meshes. *Fluids*, 4(1), 18.
 19. Huang, J.; Hu, J.; Li, S.; Wang, B.; Xu, Y.; Liang, B.; and Liu, D. (2019). Effects of physical forcing on summer time hypoxia and oxygen dynamics in the Pearl River Estuary. *Water*, 11(10), 2080.
 20. Kuang, C.; Sun, B.; Liu, S.; Gu, J.; and Yu, W. (2009). Approach of moving boundary and its application in 3D tidal current simulation of Changjiang (Yangtze) River Estuary based on ECOMSED model. *Acta Oceanologica Sinica*, 28(4), 78-85.
 21. HydroQual, Inc. (2002). *A primer for ECOMSED*, user's manual (version 1.3). One Letbridge Plaza Mahwah, N. J. 07430, USA.

22. Muhari, A.; Imamura, F.; Arikawa, T.; Hakim, A.R.; and Afriyanto, B. (2019). Solving the puzzle of the September 2018 Palu, Indonesia, tsunami mystery: clues from the tsunami waveform and the initial field survey data, *Disaster Letter*, 13, 1-3.
23. Lutfi, M. (2018). The effect of gravitational field on brachistochrone problem. *Journal of Physics: Conference Series*, 1028(1), 012060.
24. Blumberg, A.F.; and O'Neil, S. (2004). *ECOMSED A three-dimensional hydrodynamic and sediment transport model, model setup and simulations*. MacArthur Blvd Mahwah, N. J. 07430, USA.
25. Guan, H.; Dong, X.; Xue, C.; Luo, Z.; Yang, H.; and Wu, T. (2019). Optimization of POM based on parallel supercomputing grid cloud platform. *2019 Seventh International Conference on Advanced Cloud and Big Data (CBD)*, IEEE, 49-54.
26. Radjawane, I.M.; and Riandini, F. (2009). Numerical simulation of cohesive sediment transport in Jakarta Bay. *International Journal of Remote Sensing and Earth Sciences*, 6(1), 65-76.
27. Mishima, T.; Yamashita, T.; Komaguti, T.; and Riandini, F. (2008). Application of simulation model for cohesive sediment transport and bottom topography changes to tidal flat. *Proceedings of hydraulic engineering*, 52, 1333-1338.
28. Koesuma, S.; and Legowo, B. (2019). Analysis of sea level rise and tidal components based on satellite altimetry Jason-2 and tide gauge data in 2008-2016 in Sunda Kelapa. *Journal of Physics: Conference Series*, 1153(1), 012016.
29. Hendri, A.; Fauzi, M.; Ahmad, R.; Ongko, A.; and Almanna, F. (2019). The simulation of the observation data in predicting tidal patterns using the Admiralty method in Dumai's harbour. *MATEC Web of Conferences*, 276.
30. Chai, T.; and Draxler, R.R. (2014). Root mean square error (RMSE) or mean absolute error (MAE)? *Geoscientific Model Development Discussions*, 7, 1525-1534.
31. Geawhari, M.A.; Huff, L.; Mhammdi, N.; Trakadas, A.; and Ammar, A. (2014). Spatial-temporal distribution of salinity and temperature in the OuedLoukkos estuary, Morocco: using vertical salinity gradient for estuary classification. *SpringerPlus*, 3(1), 643.
32. Bambang, T. (1999). *Teknik Pantai* (2nd ed.). Yogyakarta: Beta Offset.
33. Noble, M.A.; Schroeder, W.W.; Wiseman Jr., W.J.; Ryan, H.F.; and Gelfenbaum, G. (1996). Subtidal circulation patterns in a shallow, highly stratified estuary: Mobile Bay, Alabama. *Journal of Geophysical Research: Oceans*, 101(C11), 25689-25703.